

## Analysis on insulator–metal transition in yttrium doped LSMO from electron density distribution

S ISRAEL\*, S SARAVANA KUMAR, R RENURETSON, R A J R SHEEBA<sup>†</sup> and R SARAVANAN<sup>†</sup>

Department of Physics, The American College, Madurai 625 002, India

<sup>†</sup>Department of Physics, The Madura College, Madurai 625 011, India

MS received 21 August 2010; revised 12 July 2011

**Abstract.** Yttrium doped LSMO ( $\text{La}_{1-x}\text{Sr}_x\text{MnO}_3$ ) was prepared using sol–gel technique and analysed for the insulator–metal transition from charge density variation in the unit cell with respect to different stoichiometric inclusion of yttrium. X-ray powder diffraction profiles of the samples were obtained and the well known Rietveld method and a versatile tool called maximum entropy method (MEM) were used for structural and profile refinement. The charge density in the unit cell was constructed using refined structure factors and was analysed. The charge ordering taking place in the insulator–metal transition was investigated and quantified. The insulator–metal transition was found to occur when 20% of La/Sr atoms were replaced by yttrium. The changes in the charge environment have also been analysed.

**Keywords.** LSMO; X-ray diffraction; MEM; charge density; insulator – metal transition.

### 1. Introduction

Rare-earth manganites doped with alkaline-earth metals are important materials of fundamental and technological interests (Yakel 1955; Saitoh *et al* 1995; Urushibara *et al* 1995; Lyu *et al* 1998; Alexandrov and Bratkovsky 1999; Tokura and Tomioka 1999). These materials exhibit colossal magnetoresistance (CMR), which has a great potential in magnetic devices. The colossal magnetoresistive manganites are among the most studied materials in condensed matter physics (Tokura 2000). Most of the extensive research work carried out on the manganites having the general formula,  $R_{1-x}A_x\text{MnO}_3$  ( $R$ , rare earth trivalent cation,  $A$ , divalent cation), exhibits dual novel properties such as negative colossal magneto resistance and the metal–insulator (M–I) transition in the vicinity of magnetic transition. These have been explained in terms of correlation between spin, charge and orbital degrees of freedom (Vachhani *et al* 2007).

The anti ferromagnetic  $\text{LaMnO}_3$  is known as an insulator at low temperature. Alkali earth metals like Sr or Ca doped  $\text{LaMnO}_3$  i.e.  $\text{La}_{1-x}\text{Sr}_x\text{MnO}_3$  and  $\text{La}_{1-x}\text{Ca}_x\text{MnO}_3$  with a large  $x$ , are anti-ferromagnetic. They have a decreasing resistivity  $\rho$  with  $T$ . So it is also described as an insulator despite the fact that the decrease of  $\rho$  is not exponential and  $\rho$  has an order of only  $10^2 \Omega\text{-cm}$  when  $T \rightarrow 0$  (Tsai *et al* Private Communication; Arima *et al* 1993; Krishnan and Ju 1999; Xiong *et al* 1999). With  $x$  less than about 0.50 it exhibits ferromagnetic properties at low temperature and has an

increasing resistivity  $\rho$  with  $T$ , so that these manganites are described as ferromagnetic metals, though the  $\rho$  of these manganites has an order between 1 and  $10^{-3} \Omega\text{-cm}$ . This is much larger than the typical  $\rho$  of metals of an order of  $10^{-6} \Omega\text{-cm}$  at room temperature. This kind of half metallic electric behaviour makes the manganites more interesting and motivates one to study its behaviour in terms of correlations between charge and spin.

The half metallic properties of  $\text{La}_{1-x}\text{Sr}_x\text{MnO}_3$  (LSMO) are of great importance in application in spintronics. The electronic properties of LSMO, as described by the band theory are nearly half-metallic (Picket and Singh 1997; Livesay *et al* 1999) reflecting the so-called transport half-metallic behaviour (Nadgorny *et al* 2001). However, the fascinating electronic and magnetic properties of LSMO, including colossal magneto resistance, indicate that the electronic structure is more complex than the standard band theory picture (Tokura and Tamioka 1999). Banach *et al* discussed on the self-interaction corrected local spin density approximation calculation leading to the presence of half metallic state in LSMO.

Gaur and Varma (2006) worked on nano phasic LSMO prepared using sol–gel method and sintered at different temperatures ranging from 600 to  $1000^\circ\text{C}$ . It was shown that the transport and magneto resistive properties of LSMO samples strongly depend on the sintering temperature. A substantial decrease in the insulator–metal transition temperature ( $T_{\text{IM}}$ ) and an enhancement in resistivity are found on lowering the sintering temperature. Furthermore, a reduction in magnetization and a slight decrease in paramagnetic–ferromagnetic (PM–FM) transition temperature ( $T_{\text{C}}$ ) has been observed as the sintering temperature decreases. The

\* Author for correspondence (israel.samuel@gmail.com)

magneto resistance (MR) at  $T < T_c$  increases on decreasing the sintering temperature and increasing the applied magnetic field. The enhancement in MR on decreasing the sintering temperature is explained by enhanced spin-polarized tunneling by assuming an increase of the grain boundary contribution.

The  $\text{La}_{1-x}\text{Sr}_x\text{MnO}_3$  (LSMO) compound with  $x = 0.2$ – $0.4$  are interesting materials that exhibit consecutive phase transition from paramagnetic (PM) state to ferromagnetic (FM) state and then to charge-ordered (CO) state accompanied by a sharp drop in resistivity (Jankar and van Santen 1950; van Santen and Jankar 1950). Thus, LSMO is a good material that can be used in the investigation of the lattice strain effect in the PM, FM and CO states, respectively (Zheng *et al* 2007). The inclusion of transition metal element like yttrium (Y) at the La/Sr site of LSMO induces insulator–metal transition and this behaviour depends on the stoichiometric composition of Y in LSMO. This behaviour was studied on  $\text{Y}_x\text{La}_{1-x-y}\text{Sr}_y\text{MnO}_3$  with  $y = 0.3$  by Renuretsen (2007) and they have investigated also on its electrical and magnetic transport characteristics and their dependence on the stoichiometric inclusion of yttrium. They have found that zero field resistivity in the material increases as the doping concentration of Y increases. Also, it was found that the insulator–metal transition temperature decreases from 185 to 170 K when the concentration of Y increases from  $x = 0$  to 0.2 and then the same increases to 175 K when  $x$  increases to 0.3. At the same time the magneto resistance measured at room temperature shows the trend of weakening of the ferromagnetic order and increasing of magnetic disorder as the doping concentration increases. These behaviours depend very much on the ordering of charges in the lattice and are also influenced by the inclusion of Y at the lattice site of La/Sr. A chemically driven insulator–metal transition in non-stoichiometric and amorphous gallium oxide was reported by Nagarajan (2008). They have demonstrated through experimental studies and density-functional theory calculations that the conductivity jump takes place at a critical gallium concentration and it is induced by crystallization of stoichiometric  $\text{Ga}_2\text{O}_3$  within the metastable oxide matrix in chemical terms by a disproportionation.

So far, none of these works have yielded any information on the arrangement of charges that reveals reported magnetic or electric behaviour of the materials. And hence, it was proposed that the charge density analysis in the unit cell of title material  $\text{Y}_x\text{La}_{1-x-y}\text{Sr}_y\text{MnO}_3$  may give intricate details on how the charge is distributed and on changes due to the variation in concentration of dopant material Y that would have implication on the observed electric and magnetic ordering/disordering. This has motivated us to estimate the charge and to map it along the lattice in order to see how the charge actually behaves and distributes itself in contributing to ferromagnetic ordering and insulator–metal transition. Thus this work concentrates on charge density in the unit cell of the chosen material, and for that purpose, the X-ray diffraction pattern was utilized, refined and analysed using Rietveld refinement and MEM analysis.

## 2. Sample preparation

Samples of  $\text{Y}_x\text{La}_{1-x-y}\text{Sr}_y\text{MnO}_3$  ( $y = 0.3$  and  $x = 0, 0.1, 0.2, 0.3$ ) were synthesized via sol–gel method. The required amounts of high purity nitrates of La, Sr and Mn were dissolved in double distilled water to form an aqueous solution. An equal amount of ethylene glycol was added to this solution with continuous stirring. This solution was then heated on a hot plate at a temperature of 40–80°C until a dry quick brown sol was formed. This was further decomposed in an oven at 200°C to obtain a dry fluffy material. The polymeric precursor thus obtained was calcined at 600°C for 12 h. The resulting powder was ground well and pressed into pellets and sintered at 700°C for 15 h for each composition. The samples (for  $x = 0, 0.1, 0.2, 0.3$ ) are hereafter referred to as S1, S2, S3 and S4, respectively.

The prepared samples were analysed for the content of individual constituent in the material from EDAX analysis that shows the atomic weight percentage of the constituents in the sample. The resultant composition presented in table 1 confirms inclusion of yttrium in the stoichiometrically prepared samples, thus obeying the desired molecular formula. SEM micrographs of the prepared samples are presented in figure 1. These figures show grain structure of the prepared samples and the analysis of the grain size of the particles shows that for S1–S4, the size ranges from 7.8 to 10.2 nm.

## 3. XRD analysis

The powder X-ray data were collected for all the samples using X-PERT PRO (Philips, The Netherlands) X-ray diffractometer with a monochromatic incident beam, which offers pure  $\text{CuK}_{\alpha 1}$  radiation. The  $2\theta$  range of X-ray intensity data is from 5° to 75°. The raw profile of the powder diffraction pattern for yttrium doped LSMO is presented in figure 2. The X-ray diffraction data of the samples were refined for their structural and stoichiometric parameters using the well known Rietveld technique.

The Rietveld (1969) method was used for refining structural parameters (fractional coordinates, atomic displacement parameters, occupation factors and lattice parameters) using the software Jana2006 (Petricek *et al* 2000) directly from whole powder diffraction patterns. In this method, the observed profiles were matched with the profiles constructed similarly by using pseudo-voigt (Wertheim *et al* 1974) profile shape function of Thompson *et al* (1987). It was modified, to some extent, to accommodate various Gaussian FWHM

**Table 1.** EDAX analysis of the prepared samples.

Sample	$x$	La	Sr	Y	Mn	O
S1	0.0	11.96	6.93	3.56	18.72	45.28
S2	0.1	10.84	7.03	3.72	19.97	43.31
S3	0.2	8.99	9.02	4.64	19.45	38.10
S4	0.3	8.46	11.04	4.84	22.70	42.66

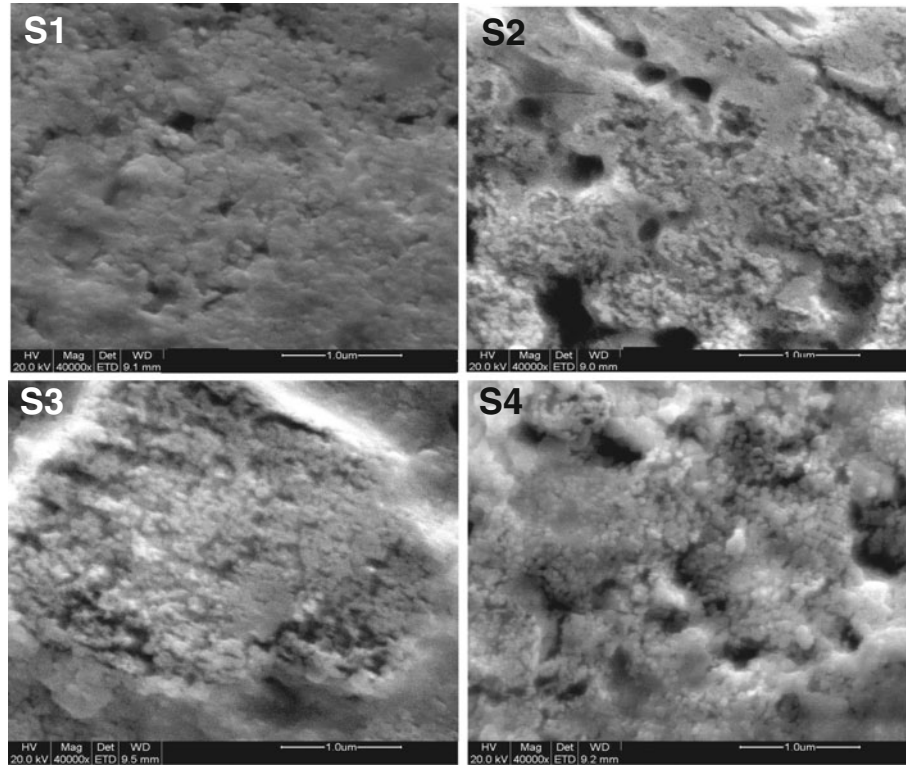


**Figure 1.** SEM micrographs of grown sample.

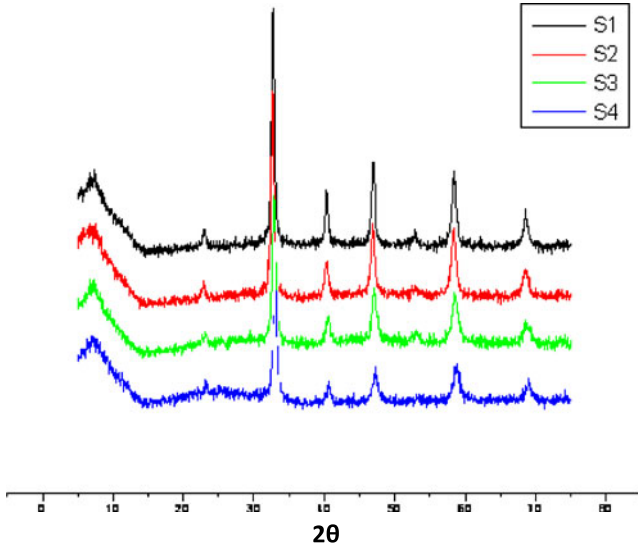


**Figure 2.** Raw powder profile for yttrium doped LSMO.

parameters and Scherrer coefficient,  $P$ , for Gaussian broadening. The profile asymmetry was also introduced by employing multi-term Simpson rule integration devised by Howard (1982). It incorporates symmetric profile shape function with different coefficients for weights and peak shift. Jana2006 also employs the correction for the preferred orientation which is independent of diffraction geometry according to the March–Dollase function (Israel *et al* 2003, 2004). The

**Table 2.** Refined structural parameters.

Sample	$x$	$a(\text{\AA})$	$b(\text{\AA})$	$c(\text{\AA})$	$\alpha$	$\beta$	$\gamma$	$V(\text{\AA}^3)$
S1	0.0	5.4913	5.4913	13.1373	90	90	120	343.0778
S2	0.1	5.5021	5.5021	13.0958	90	90	120	343.3463
S3	0.2	5.5029	5.5029	13.3420	90	90	120	349.9036
S4	0.3	5.3639	5.3639	12.1617	90	90	120	303.0365

calculated profiles thus evolved were compared with the observed ones. During the refinement, the trial cell parameters were introduced as  $a = b = 5.503 \text{ \AA}$  and  $c = 13.342 \text{ \AA}$  for all the samples. The position of the atoms for La, Sr and Y was taken as (0, 0, 0.25) with relevant stoichiometric compositions and for oxygen (0.4592, 0, 0.25) whereas Mn atoms were placed at the origin. The symmetric group of  $R-3c$  was used for positioning the atoms in the unit cell. The raw intensities thus refined have yielded structural parameters, structure factors and the reliability indices that are presented in tables 2, 3 and 4, respectively. The refined cell parameters show inconsistent and slight variation in the size of unit cell in all three dimensions and they are found to decrease in  $\vec{a}$  and  $\vec{b}$  directions as the concentration ( $x$ ) of yttrium increases from 0 to 0.2 and then decreases to 0.3. In  $\vec{c}$  direction the cell length decreases for S1 and S2 and increases for S2 and again decreases from thereon. The list of refined structure factors (table 3) is considered to be very accurate as evidenced from the  $R$ -factors presented in table 4. Successful refinement has

**Table 3.** Comparison of observed and calculated structure factors.

<i>h</i>	<i>k</i>	<i>l</i>	<i>S1</i>		<i>S2</i>		<i>S3</i>		<i>S4</i>	
			<i>F<sub>o</sub></i>	<i>F<sub>c</sub></i>	<i>F<sub>o</sub></i>	<i>F<sub>c</sub></i>	<i>F<sub>o</sub></i>	<i>F<sub>c</sub></i>	<i>F<sub>o</sub></i>	<i>F<sub>c</sub></i>
1	−1	2	95.5572	96.3961	86.6512	87.0058	77.8699	77.9434	68.3951	68.3738
2	−1	0	295.328	295.013	285.560	286.677	278.737	278.649	267.482	267.502
1	0	4	297.418	296.976	287.144	288.249	282.005	281.905	264.702	264.680
2	−1	3	28.2633	28.2628	28.1630	28.2642	28.4125	28.4047	27.2161	27.2016
2	0	2	182.862	182.130	174.415	175.053	168.447	168.330	157.268	157.274
0	0	6	185.414	186.134	177.916	178.543	174.290	174.141	154.874	155.013
2	−2	4	326.526	325.907	317.875	319.008	314.345	314.412	293.373	294.191
3	−1	1	19.5249	19.4502	19.4206	19.4898	19.5152	19.5027	18.7830	18.7856
3	−2	2	75.5782	75.3550	68.8895	69.1350	63.1662	63.1185	56.0730	56.0786
2	−1	6	70.1936	69.9832	63.4575	63.6837	58.0163	58.0251	50.0972	50.1397
3	0	0	211.748	211.670	205.364	206.096	200.578	200.575	189.542	189.665
3	−1	4	204.156	204.031	197.504	198.208	193.604	193.571	179.850	179.707
1	−1	8	198.941	198.648	191.517	192.200	190.201	190.126	167.482	167.515
3	−2	5	14.6794	14.6628	14.6096	14.661	14.8003	14.8137	13.6154	13.6231
4	−2	0	214.601	214.723	209.407	210.154	204.792	205.476	193.485	193.438
2	0	8	216.475	216.201	209.925	210.673	209.351	209.910	184.017	183.973
4	−3	1	22.5998	22.6081	22.5967	22.6772	22.7204	22.6919	21.5309	21.5292
4	−2	3	1.5746	1.5752	1.5732	1.5788	1.5863	1.5843	1.4870	1.4863
3	−1	7	11.4185	11.4350	11.3746	11.4152	1.6280	11.6205	10.2974	10.3141
4	−1	2	54.8408	54.9391	50.1553	50.3341	45.8521	45.8632	40.3267	40.3690
2	−1	9	12.0419	12.0602	11.9590	12.0017	12.3588	12.3563	10.5008	10.5058
3	0	6	62.9367	63.0213	58.2374	58.4450	54.3628	54.4375	47.2866	47.3613
3	−3	6	62.9367	63.0213	58.2374	58.4450	54.3628	54.4375	47.2866	47.3613
1	0	10	56.2390	56.4029	51.5207	51.7044	48.1100	48.2084	39.8383	39.9141
4	−3	4	144.025	143.709	138.947	139.442	135.594	135.839	124.442	124.563
3	−2	8	145.425	145.272	140.118	140.617	138.280	138.726	121.325	121.441
4	−1	5	18.0292	18.0646	18.0224	18.0867	18.2807	18.2399	16.6113	16.6976
4	−4	2	79.9734	80.0271	76.0547	76.3240	72.8263	72.6623	65.5644	65.8734
4	−2	6	81.4756	81.4257	77.3363	77.6072	74.7161	74.5585	65.4907	65.6741
2	−2	10	84.2207	84.4012	80.0429	80.3266	78.6561	78.6057	64.9800	65.3251
4	0	4	151.976	151.592	147.519	148.044	145.131	145.093	132.224	132.654
0	0	12	153.769	153.674	148.457	148.958	150.881	150.930	121.712	121.856
5	−2	1	6.2839	6.2724	6.2743	6.2955	6.2953	6.2996	5.9092	5.9177
4	−3	7	14.7651	14.7481	14.6962	14.7439	14.9548	14.9643	13.2727	13.3047
5	−3	2	52.0971	52.1265	48.6049	48.7626	45.4483	45.4576	40.3050	40.3264
3	−1	10	45.3467	45.7055	42.0398	42.1610	39.5644	39.6056	32.4068	32.4676
5	−1	0	110.637	110.846	107.523	107.772	104.350	104.610	96.1356	96.2437
5	−2	4	114.441	114.647	111.277	111.502	108.527	108.773	98.4834	98.6904
4	−1	8	105.568	105.778	102.144	102.321	100.448	100.665	87.2640	87.3380
2	−1	12	103.615	104.110	100.067	100.223	100.273	100.422	79.6385	81.1179
5	−4	3	10.7475	10.8279	10.8444	10.8638	10.8652	10.8947	10.0968	10.1056
5	−1	3	10.7475	10.8279	10.8444	10.8638	10.8652	10.8947	10.0968	10.1056
5	−3	5	5.1611	5.2023	5.2063	5.2131	5.2353	5.2509	4.7739	4.7883
4	−2	9	0.8512	0.8542	0.8507	0.8524	0.8702	0.8717	0.7385	0.7498
3	−2	11	6.2899	6.2288	6.1903	6.1970	6.3937	6.4058	5.1980	5.2903
4	−4	8	110.117	111.064	108.061	108.117	107.089	107.015	90.6055	92.6618
5	−2	7	4.3710	4.3757	4.3791	4.3789	4.4067	4.4357	3.9145	3.9419
5	0	2	43.8468	43.8146	41.2971	41.3065	38.6118	38.8085	33.8864	34.2335
5	−4	6	36.9237	37.0150	34.3686	34.3925	31.9058	32.0588	27.0787	27.2534
5	−1	6	36.9237	37.0150	34.3686	34.3925	31.9058	32.0588	27.0787	27.2534
4	−3	10	34.0192	34.1100	31.3905	31.4003	29.2404	29.4186	23.5978	23.6972
1	−1	14	34.5234	34.5481	31.7058	31.7523	30.2643	30.4237	—	—
6	−3	0	80.3822	80.4326	78.0268	78.0845	75.0460	75.6357	68.3584	68.6517
5	−5	4	89.4474	89.4923	86.9918	87.1434	84.3891	85.0433	76.0025	76.3512
5	−3	8	85.4306	85.4650	82.7942	82.8835	80.9747	81.6455	—	—



**Table 3.** (continued.)

<i>h</i>	<i>k</i>	<i>l</i>	<i>S</i> 1		<i>S</i> 2		<i>S</i> 3		<i>S</i> 4	
			<i>F</i> <sub>o</sub>	<i>F</i> <sub>c</sub>	<i>F</i> <sub>o</sub>	<i>F</i> <sub>c</sub>	<i>F</i> <sub>o</sub>	<i>F</i> <sub>c</sub>	<i>F</i> <sub>o</sub>	<i>F</i> <sub>c</sub>
3	−3	12	82.0722	82.1059	79.1405	79.1891	78.7130	79.3163	—	—
3	0	12	82.0722	82.1059	79.1406	79.1891	78.7130	79.3163	—	—
6	−4	1	1.7452	1.7465	1.7541	1.7542	1.7423	1.7553	—	—
6	−3	3	12.0192	12.0364	12.0812	12.0828	12.0207	12.1140	—	—
6	−2	2	43.3766	43.4030	41.2220	41.2683	—	—	—	—

**Table 4.** List of reliability indices (%) after final Rietveld refinement.

<i>R</i> -factors	<i>S</i> 1	<i>S</i> 2	<i>S</i> 3	<i>S</i> 4
<i>R</i> <sub>obs</sub> (%)	0.20	0.30	0.19	0.23
<i>wR</i> <sub>obs</sub> (%)	0.32	0.29	0.32	0.39
<i>R</i> <sub>all</sub> (%)	0.20	0.30	0.19	0.23
<i>wR</i> <sub>all</sub> (%)	0.32	0.29	0.32	0.39
<i>R</i> <sub>p</sub> (%)	7.29	8.49	4.24	4.13
<i>wR</i> <sub>p</sub> (%)	9.83	11.61	5.65	6.03

yielded low *R*-factors. This determines the accuracy of the data and their utility in calculating accurate charge density in the unit cell.

It has been proved that there is interplay between electronic and structural transition in LSMO system by Bindu *et al* (2008) who have investigated on the evolution of distortion in the lattice of La<sub>0.2</sub>Sr<sub>0.8</sub>MnO<sub>3</sub> using Mn *k*-edge extended X-ray absorption fine structure (EXAFS). They have found that a remarkable evolution of distortion takes place across phase transition while the system is treated between 12 K and 300 K. The results show the fluctuation in Mn 3*d* orbital occupancy during the phase transition and its implication on the electronic property of the system, the orbital and spin ordering. It is known (Bindu *et al* 2008) that in a system like La<sub>1−*x*</sub>Sr<sub>*x*</sub>MnO<sub>3</sub> (*x* < 0.5) when Mn–O–Mn angle becomes close to 180°, the Mn-*e<sub>g</sub>* orbitals become almost degenerate (Maezono *et al* 1998; van den Brink *et al* 2009). This degeneracy strongly depends on the local structure of MnO<sub>6</sub> octahedra. Any distortion in this octahedra has an implication on the electronic properties and hence the charge and the spin ordering of the chosen material (Bindu *et al* 2008). When the octahedra is compressed along the apical direction, the *d*-orbital (*d<sub>x<sup>2</sup>−y<sup>2</sup></sub>*) corresponding to the plane having Mn–O bond length will be more populated compared to the perpendicular one. Also, the strong influence of disorder in Mn–O shorter bond length that leads to hybrids in the electronic states was found to be a reason for the insulating transport in addition to the formation of zener polaron wherein a conduction electron gets trapped in between two Mn sites leading to a polaronic distortion. These observations indicate the relationship between the electronic properties and a change in the Mn–O bond length that leads to a significant fluctuation in the occupancy of Mn *e<sub>g</sub>*-orbitals.

In the present work also, we have attempted to find a relationship between the structural distortion and the electronic properties. Beforehand, the structural investigation on the bond length in our system Y<sub>*x*</sub>La<sub>1−*x*−*y*</sub>Sr<sub>*y*</sub>MnO<sub>3</sub> (*y* = 0.3) shows that Mn–O bond length has become shorter as *x* is increased from 0 to 0.3. An analysis on bond length shows that La/Sr/Y–O bonds are of three types whereas O–O has two bond lengths of which one is similar to La–O. In all the cases, the bond lengths have decreased as the composition Y in the system increases which may be attributed to the smaller size of replacement metal Y whose *r<sub>i</sub>* = 1.02 Å compared to *r<sub>i</sub>*(La) = 1.16 Å and *r<sub>i</sub>*(Sr) = 1.26 Å. Also, the angle between La–O–La is found to be sharply decreasing from 180° when *x* = 0 till *x* = 0.3 except for the system *x* = 0.2 for which the angular distortion is more than that for the systems when *x* = 0.1 or 0.3. Similar type of distortion has been observed in the arrangement of MnO<sub>6</sub> octahedra where Mn–O–Mn angle shows a decreasing behaviour starting from *x* = 0 till *x* = 0.3 except for the system *x* = 0.2 (see figures 3 and 4). Thus, the distortion in *x* = 0.2 is unique and therefore, it is expected that the interplay between the structural distortion at *x* = 0.2 and the electronic property of this stoichiometric composition is an important one to be investigated.

#### 4. Charge density determination using MEM

The structure factors extracted from the refinement were further utilized to calculate the accurate charge density in the unit cell using maximum entropy method (MEM). MEM is a very good tool for the estimation of accurate charge density and is a statistical approach proposed by Collins (1982). MEM method depends heavily on the observed information and when the information is accurate, it can be used for the reconstruction of charge density accurately and hence is known to be highly unbiased. MEM gives positive charge density everywhere and hence it gives the true charge density that can be directly analysed for any charge related properties.

In the MEM refinement, for the construction of charge density, the unit cell was divided into 54×54×144 pixels and each pixel was filled with prior density equal to *F*<sub>000</sub>/*V*. The prior density was initially used for the construction of structure factors, which would then be compared with the observed structure factors. The error in the difference in

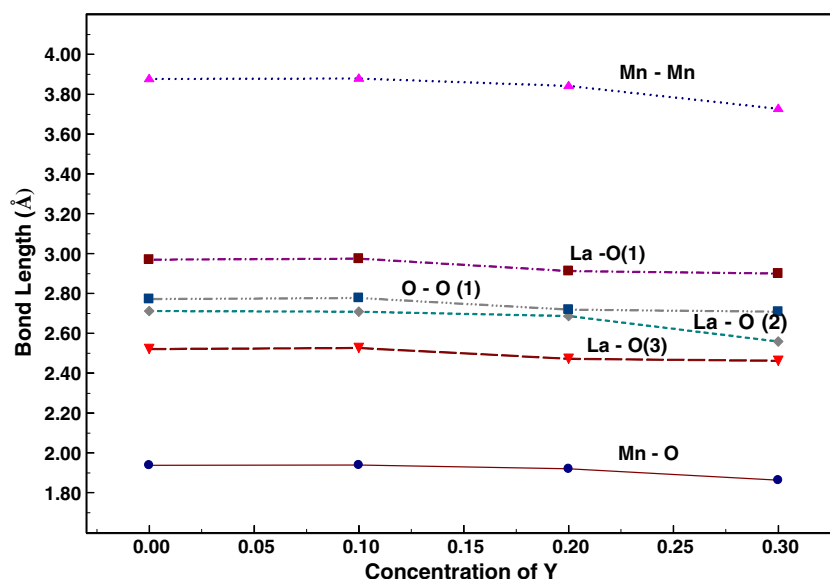


Figure 3. Graph drawn between bond length and concentration of Y.

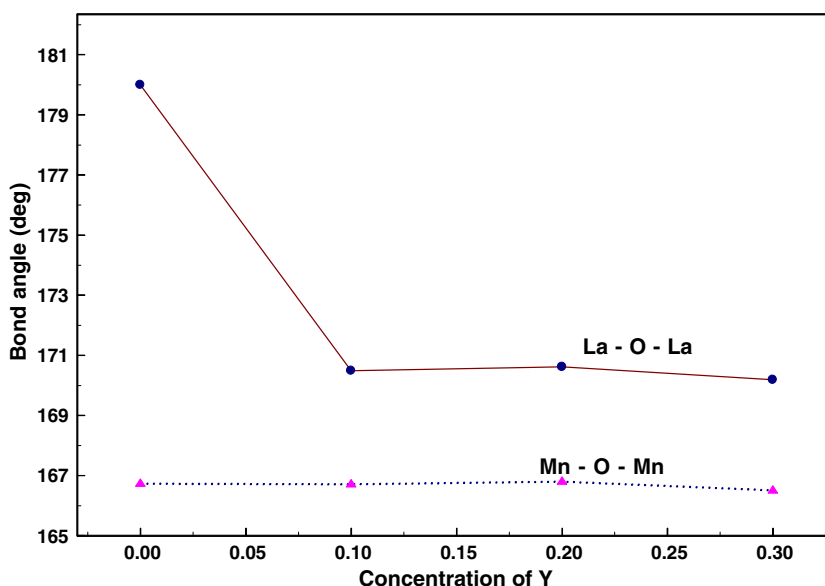


Figure 4. Graph drawn between bond angle and concentration of Y.

the structure factors was again added to the calculated ones and thus the entropy was increased. The process of increasing the entropy in the structure factors as well as in the charge density was done iteratively. The iteration would stop when the soft criterion 'C' became 1. At this situation, the observed structure and MEM refined structure would match. The charge density constructed at this juncture using the structure factors was called the desired MEM charge density. The unique feature of this charge density is that it is real and positive. This charge density gives an accurate picture of the distribution of charges in the unit cell, which is then analysed for bonding and charge related properties of the material. The

detailed methodology adopted here and the definition of the criterion used is presented in detail by Syed Ali *et al* (2006).

In the present work, MEM refined structure factors were elucidated using the software called PRIMA (Izumi and Dilanian 2002; Ruben and Fujio 2004) (A FORTRAN program to determine electron density by MEM from X-ray data). The parameters used in this refinement and the reliability indices were tabulated in table 5. The phase factors evaluated by MEM and listed in table 6 were then used in the construction of the charge density in the unit cell and then visualized with the help of the visualization software called VESTA (Momma and Izumi 2008).

**Table 5.** MEM refinement parameters.

Parameters	S1	S2	S3	S4
Number of pixels in the unit cell	419904	419904	419904	419904
Number of electrons in the unit cell	602	591	580	569
$\lambda$	0.00760	0.00633	0.00845	0.00816
Number of refinement cycles	1776	2128	1445	1325
$C$	0.99905	0.99977	0.99899	0.99946
$R_F$	0.01153	0.01140	0.01179	0.01264
$wR_F$	0.01073	0.01006	0.01120	0.01162

**Table 6.** MEM refined structure factors.

$h$	$k$	$l$	S1		S2		S3		S4	
			$F_{\text{obs}}(R)$	$F_{\text{MEM}}(R)$	$F_{\text{obs}}(R)$	$F_{\text{MEM}}(R)$	$F_{\text{obs}}(R)$	$F_{\text{MEM}}(R)$	$F_{\text{obs}}(R)$	$F_{\text{MEM}}(R)$
1	-1	2	-96.86400	-97.42980	-87.71910	-88.17093	-78.64830	-79.00253	-96.8640	-97.4298
2	-1	0	298.88501	289.23495	291.00800	281.60672	282.88501	274.01306	298.8850	289.2349
1	0	4	300.84201	290.67667	292.56500	282.78946	286.14499	276.39368	300.8420	290.6766
2	-1	3	-27.99340	-27.95404	-28.00730	-27.96641	-28.14740	-28.10325	-27.9934	-27.9540
2	0	2	-182.86099	-178.76613	-175.75999	-171.98723	-168.75700	-165.15172	-182.8609	-178.7661
0	0	6	-186.82401	-186.59293	-179.20000	-179.02831	-174.52000	-174.27673	-186.8240	-186.5929
2	-2	4	329.13699	315.14847	322.62900	309.11227	317.89999	304.28735	297.38000	284.93732
3	-1	1	-19.22180	-19.22282	-19.27180	-19.27345	-19.28460	-19.28562	-18.57040	-18.57231
3	-2	2	-75.58720	-75.78486	-69.63100	-69.78431	-63.64960	-63.77489	-56.56120	-56.69661
2	-1	6	-70.10670	-70.25644	-64.10100	-64.21288	-58.51450	-58.61178	-50.60690	-50.69991
3	0	0	214.11600	216.75276	209.00500	211.49831	203.47400	205.95647	192.45100	195.03755
3	-1	4	206.41299	207.57643	201.05800	202.15709	196.43900	197.47969	182.42400	183.64667
1	-1	8	200.95900	203.95462	194.96700	197.84657	192.96300	195.81483	170.06100	172.60799
3	-2	5	-14.45690	-14.46274	-14.46530	-14.47051	-14.61660	-14.62308	-13.43240	-13.43704
4	-2	0	216.75200	219.73764	212.59300	215.57376	207.87199	210.82867	195.68100	198.66862
2	0	8	218.16400	220.99138	213.02699	215.86336	212.26199	215.02055	186.00600	188.45009
4	-3	1	22.24550	22.26476	22.33100	22.34970	22.34560	22.36598	21.19090	21.21136
3	-1	7	11.24940	11.25021	11.23830	11.23935	11.44220	11.44312	10.14520	10.14624
4	-1	2	-54.95140	-54.98779	-50.62730	-50.66242	12.16600	12.17008	-40.75810	-40.82626
2	-1	9	11.86290	11.86549	11.81390	11.81588	-46.24320	-46.28590	10.32920	10.33013
3	0	6	-63.17850	-63.16367	-58.82340	-58.81057	-54.84450	-54.84830	-47.70440	-47.69479
3	-3	6	-63.17850	-63.15493	-58.82340	-58.79358	-54.84450	-54.82763	-47.64478	-47.70440
1	0	10	-56.46470	-56.44242	-52.02240	-52.00417	-48.60000	-48.59296	-	-
4	-3	4	145.10500	147.08804	141.29100	143.18825	137.76601	139.70868	126.41100	128.17938
3	-2	8	146.66901	148.35056	142.45000	144.07030	140.65900	142.33714	123.18600	124.33186
4	-1	5	17.73780	17.74450	17.77480	17.78078	17.92680	17.93577	16.39790	16.40396
4	-4	2	-80.19090	-80.31269	-76.59610	-76.71651	-72.85230	-72.98491	-65.92040	-65.98716
4	-2	6	-81.57540	-81.80088	-77.85800	-78.04697	-74.72410	-74.97234	-65.68830	-65.83702
2	-2	10	-84.51670	-84.60294	-80.52980	-80.61889	-78.71670	-78.82734	-	-
4	0	4	152.81200	154.17598	149.65300	150.64201	146.72501	148.01175	134.16299	135.37238
0	0	12	154.81500	154.75652	150.45599	150.33879	152.50101	152.46671	123.09400	122.89851
5	-2	1	-6.14820	-6.14847	-6.17680	-6.17708	-6.18080	-6.18113	-5.80280	-5.80310
4	-3	7	-14.45350	-14.45702	-14.46300	-14.46594	-14.68110	-14.68541	-13.03920	-13.04132
5	-3	2	-52.20320	-52.20442	-49.03220	-49.03365	-45.75120	-45.74759	-40.57240	-40.53955
3	-1	10	-45.71270	-45.68018	-42.39300	-42.36577	-39.90720	-39.87333	-32.73680	-32.70523
5	-1	0	111.66900	111.57355	109.00600	108.85495	105.92900	105.90720	97.53930	97.49493
5	-2	4	115.50400	115.40400	112.75800	112.59232	110.10900	110.08731	99.96580	99.75921
4	-1	8	106.53200	106.27540	103.48100	103.18642	101.94900	101.76045	88.51510	87.79919
2	-1	12	104.83400	104.61339	101.34000	101.08974	101.69300	101.59943	82.17420	81.36272
5	-4	3	10.59540	10.59474	10.64160	10.64126	10.67210	10.67095	9.89260	9.89177
5	-1	3	10.59540	10.59496	10.64160	10.64130	10.67210	10.67123	9.89260	9.89211
5	-3	5	-5.09030	-5.09069	-5.10620	-5.10673	-5.14350	-5.14405	-4.68660	-4.68711
3	-2	11	6.09290	6.09283	6.06780	6.06768	6.27400	6.27383	5.17290	5.17155

Table 6. (continued.)

$h$	$k$	$l$	S1		S2		S3		S4	
			$F_{\text{obs}}(R)$	$F_{\text{MEM}}(R)$	$F_{\text{obs}}(R)$	$F_{\text{MEM}}(R)$	$F_{\text{obs}}(R)$	$F_{\text{MEM}}(R)$	$F_{\text{obs}}(R)$	$F_{\text{MEM}}(R)$
4	-4	8	111.74100	111.62278	109.14400	108.94328	108.11100	107.86006	93.62620	93.23278
5	-2	7	4.27480	4.27440	4.28260	4.28244	4.33860	4.33807	3.85180	3.85135
5	0	2	-43.82500	-43.82561	-41.47720	-41.47675	-38.99490	-38.99964	-34.37440	-34.35764
5	-4	6	-36.96990	-36.93555	-34.55060	-34.52811	-32.28200	-32.24652	-27.46640	-27.43681
5	-1	6	-36.96990	-36.99049	-34.55060	-34.56697	-32.28200	-32.29472	-27.46640	-27.47366
4	-3	10	-34.02210	-34.00004	-31.53300	-31.51783	-29.64120	-29.61264	-23.91730	-23.92012
1	-1	14	-34.47770	-34.47681	-31.88820	-31.88782	-30.64360	-30.63927	—	—
6	-3	0	80.78130	80.46512	78.81040	78.57000	76.47470	75.88114	69.50410	69.06966
5	-5	4	89.95310	89.71677	87.95710	87.79597	85.94180	85.50450	77.21370	76.82559
5	-3	8	85.88150	85.42356	83.65330	83.29661	82.52440	81.93040	—	—
3	-3	12	82.47800	82.39244	79.90820	79.86161	80.17340	79.95887	—	—
3	0	12	82.47800	82.22469	79.90820	79.73746	80.17340	79.59299	—	—
6	-3	3	-11.74420	-11.74210	-11.80330	-11.80133	-11.83410	-11.82994	—	—
6	-2	2	-43.38010	-43.32754	-41.37450	-41.33142	-39.21420	-39.12542	—	—

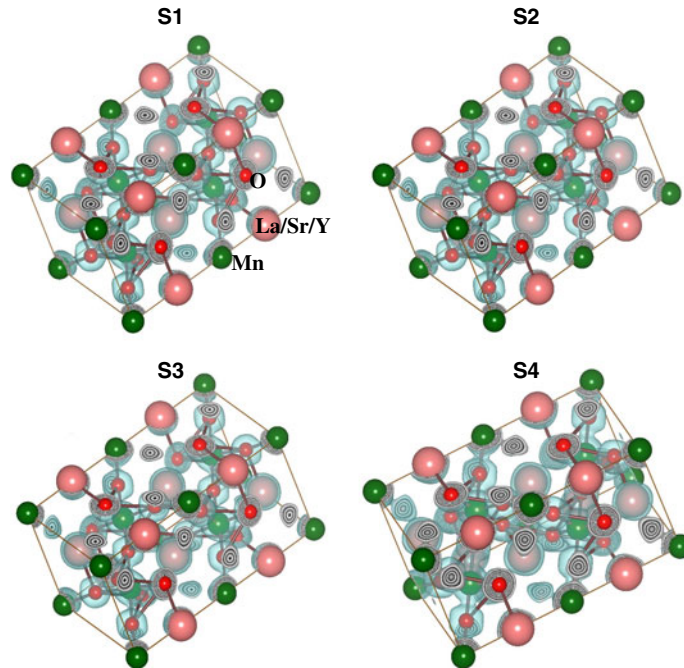


Figure 5. Three dimensional charge density in unit cell.

The charge density in the unit cell is drawn in 3-dimension for all the four samples in ball and stick model of structure and is presented in figure 5. Two dimensional miller planes are also mapped for the understanding of the bonding behaviour between Mn–O, La–O and O–O atoms and are presented in figures 6–8. One dimensional charge density profiles between the atoms are drawn to quantify the bonding character and are presented in figure 9.

The three dimensional picture of charge density with iso-surface level,  $0.5 \text{ e}/\text{\AA}^3$ , for all the samples presented in figure 5 shows the arrangement of charges and their variations with respect to the concentration of dopant material yttrium at the

lattice site of La. These pictures show that the inclusion of Y reduces the size of charge sphere of La and is primarily due to the fact that the ionic radius of Y ( $r_i = 1.02 \text{ \AA}$ ) is smaller than that of La ( $r_i = 1.16 \text{ \AA}$ ). The reduction in the size of the charge sphere due to the inclusion of Y does not reflect on the global change in the lattice parameters while the angles La–O–La have been largely modified and also the  $\text{MnO}_6$  octahedra has been rearranged to include changes due to distortion. Indeed, the change in the cell dimensions can actually be attributed to the change in the electronic properties of the material particularly on a system with  $x = 0.2$ . While including Y in the lattice it has primarily rearranged



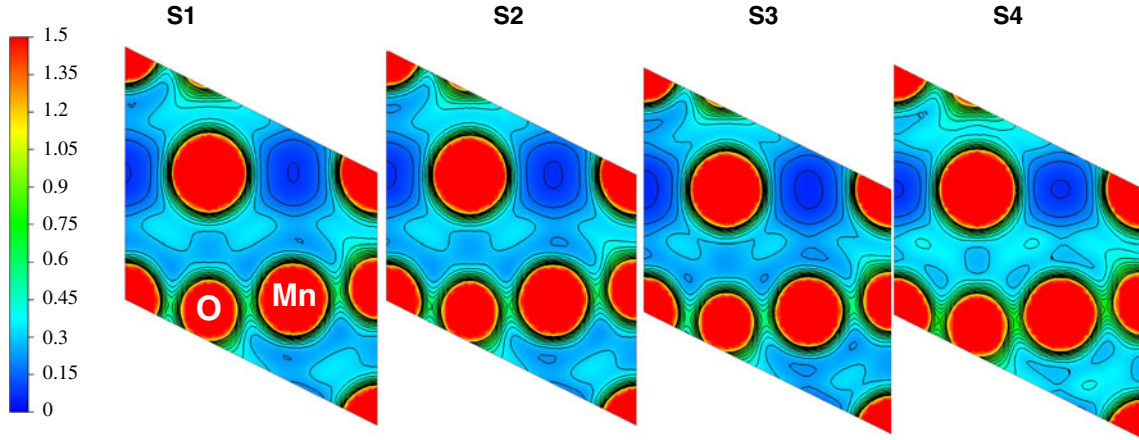


**Figure 6.** Two dimensional miller map showing Mn–O bond in (1 0 4) plane. Contour lines are also drawn between 0 to  $1.5 \text{ e}/\text{\AA}^3$  with  $0.1 \text{ e}/\text{\AA}^3$  interval.

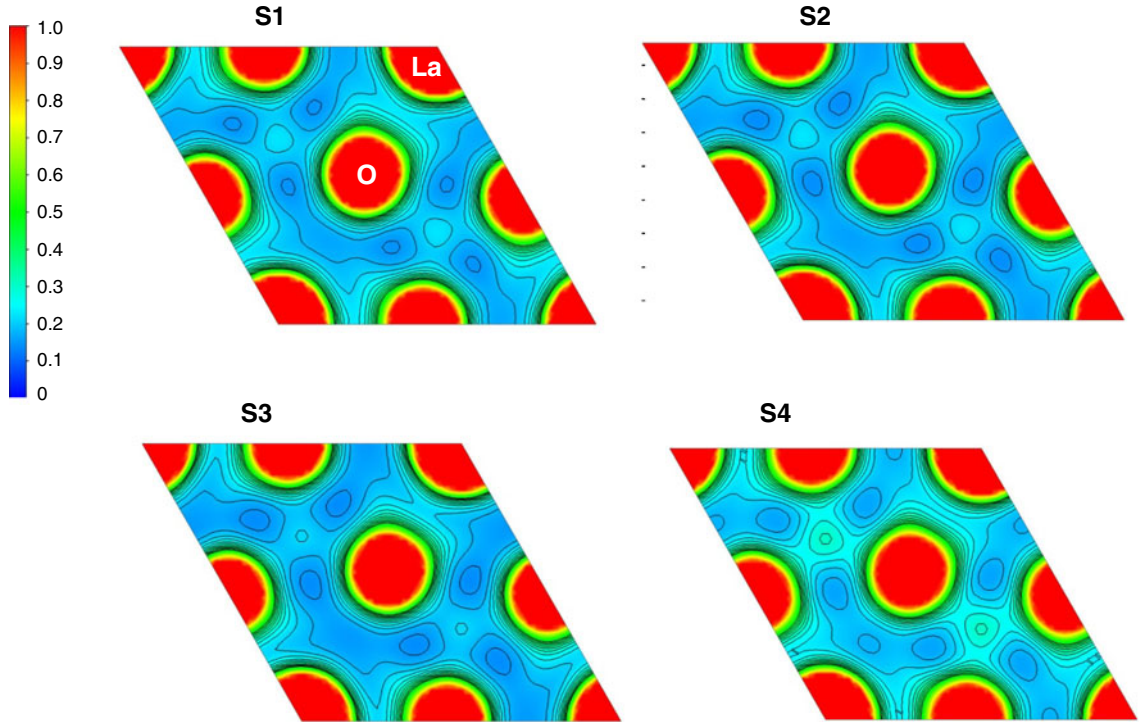


**Figure 7.** Two dimensional miller map showing La–O bond in (0 0 4) plane. Contour lines are also drawn between 0 to  $1 \text{ e}/\text{\AA}^3$  with  $0.06 \text{ e}/\text{\AA}^3$  interval.

the charge density distribution such that the changes in the cell dimensions are small. Thus figure 5 explains the change in cell dimensions as found in table 2 and also evidences the inclusion of Y in the samples.

## 5. Insulator–metal transition

Metal–insulator transition is a transition characterized by a sudden change in electrical transport properties (conductivity) due to a reversible change from localized to itinerant behaviour of the electrons. Doping a material can change

its internal electronic structure, giving rise to or eliminating bandgaps. Materials in which a bandgap prohibits electronic conductivity are called bandgap insulators. Electron–electron interaction can also lead to the opening of an interaction-induced gap, the so-called Mott–Hubbard gap. Disorder in the material composition can lead to Anderson localization which prohibits conductivity. This is a disorder-induced metal–insulator transition even without any bandgap.

A metal–insulator transition is primarily characterized by the localization of the charge carriers, which prevent them from transporting electric current. The two basic mechanisms that cause electron localization are the correlations

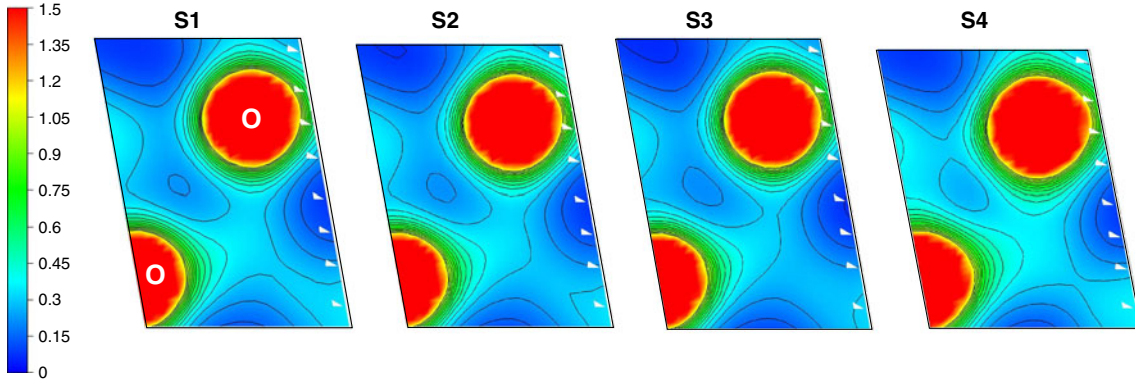


**Figure 8.** Two dimensional miller map showing O–O bond in (2 2 1) plane. Contour lines are also drawn between 0 to  $1.5 \text{ e}/\text{\AA}^3$  with  $0.1 \text{ e}/\text{\AA}^3$  interval.

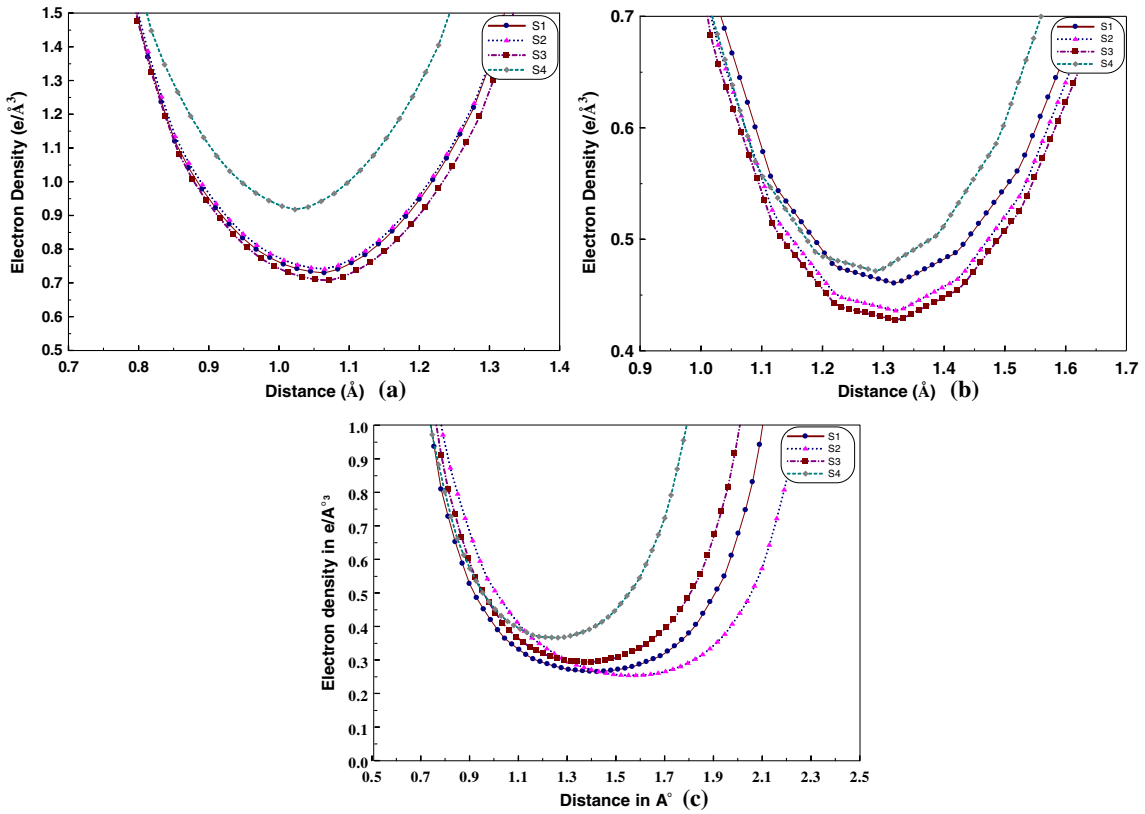


**Figure 9.** One dimensional electron density profile along (a) Mn–O bond, (b) La–O bond and (c) O–O bond.

among the electrons and the disorder present in the sample. Mott demonstrated that electron–electron interactions can produce a metal–insulator transition even in a system without disorder (Mott 1974). Anderson discovered that a disorder, such as strong spatial fluctuations in the electrostatic potential caused by impurities, can drive a metal insulator transition in a system of non-interacting electrons (Anderson 1958). The theoretical description of the situation, when both effects are present is a central unsolved problem, especially when the electron–electron interactions are strong.

The occurrence of insulator–metal transition and then a metal–insulator transition due to the inclusion of dopant material (Y) in the stoichiometrically synthesized LSMO is a very interesting phenomenon that should be analysed with experimental tools. The electrical transport property of the material has pronounced that the insulator–metal–insulator transition happens at the composition ratio  $x = 0.2$  for the chosen material and this can be investigated in the charge density route. The charge density mapping is bound to give minute details about the localization and delocalization of

the charges between the atoms when bonded. Also the effect of spatial distribution of charges from neighbouring atoms can affect the environment which leads to a change in the behaviour of localizing the charges. Thus it is expected that the presence of Y in some of the lattice sites of La/Sr can induce the transition from metal/insulator to insulator/metal. The investigation of charge localization/delocalization can be done on mapping the charges in the valence region preferably in the bonding directions. It is known that the estimation of charges in the closed shell interaction (ionic) will have charges to have a perfect saddle at the mid-bond position and is low compared to the shared shell interaction (metallic/covalent) for which the mid bond will be enacted by a flattened localized charge distribution with a high charge density. This is the prime indicator that will lead to the finding of the ionic to metal transition which is otherwise called insulator–metal transition. The necessary tools for these investigations are accurate 2-D and 1-D charge density profiles.

To understand the Mn–O bonding and the charge localization between them (1 0 4) plane is drawn on the unit cell with contour levels between 0 and  $1.5 \text{ e}/\text{\AA}^3$  at an interval of  $0.1 \text{ e}/\text{\AA}^3$  and is presented in figure 6. Figure 6 shows bonding between Mn–O being predominantly ionic with partial covalent character and hence a large localized charge density of about  $0.8 \text{ e}/\text{\AA}^3$  is found to be present at the mid bond position. But strength of the ionicity is found to vary with respect to the charge environment at the lattice site of La. The difference in the electro negativity between Mn–O induces ionicity in the bond with a partial covalent character and this is enhanced more due to the inclusion of Y in the lattice site of La. The effect of dopant material (Y) on the  $\text{MnO}_6$  polyhedra is felt in the lattice between Mn–O and thus effectively reducing the ionicity while increasing the localized charge in the middle as the concentration of Y increases. Though the inclusion of Y in the lattice site of La does not alter the bonding nature between Mn and O, it affects strength of the bond. The magnitude of the intermediate charge between Mn and O is found to vary alternatively for different stoichiometric compositions showing different strengths of the bond due to the doping effect (see table 7).

The effect of Y on the bonding between La–O can be understood from the charge density mapping upon (0 0 4) plane in the unit cell. This is drawn with the contour level between 0 to  $1 \text{ e}/\text{\AA}^3$  with  $0.06 \text{ e}/\text{\AA}^3$  as the interval. As the difference in electro negativity between La/Sr and O is large the ionic character is well pronounced between these atoms

and the maps (figure 7) also show that a perfect ionic character exists in the bonding. But this ionic character is found to increase as  $x$  increases to 0.2 where the delocalization of the charges takes place. The ionic character decreases from then on as  $x$  increases from 0.2 and this leads to the localization or accumulation of charges between the atoms. These behaviours are well pronounced in figure 7. The decrease in ionic character can be attributed to the introduction of metallic character in the system and thus any decrease in the ionicity can be ascribed to the increase in the metallicity in the system. The bond critical points (BCP) and the charge density at BCP presented in table 7 quantify the above argument. Here,  $x = 0.2$  is found to be the transition point where the system makes transition from insulator to metallic.

The bonding between O–O is observed in the plane (2 2 1) drawn at a distance of  $1.6 \text{ \AA}$  from the origin and between the contour level of 0 to  $1.5 \text{ e}/\text{\AA}^3$  with  $0.1 \text{ e}/\text{\AA}^3$  as interval and is presented here in figure 8. This figure shows the covalent non-polar bonding between the oxygen atoms with the mid bond smeared owing to thermodynamic effects. The covalent charge is found to lie in a curved bond path and this introduces the so called spatial disorder, such as strong spatial fluctuations in the electrostatic potential, caused by impurities that can drive a metal/insulator to insulator/metal transition in a system of non-interacting electrons as explained by Anderson (1958). The curved bond path shown in figure 8 is the prime evidence that describes the spatial disorder in the lattice. The magnitude of the covalent charge seems to increase as  $x$  increases up to 0.2 and drops when  $x = 0.3$ . This behaviour again evidences the fact that the spatial disorder of charges and hence the insulator – metal transition happens at  $x = 0.2$ .

The investigation on the bonding between La/Sr and O shows that the ionicity increases from  $x = 0$  to 0.2 and then decreases from thereon and the same trend was again observed in the covalent non-polar bonding between O–O as evidenced from figure 8. The same behaviour was evidenced from the one dimensional charge density profile drawn between the atoms presented in figure 9. The quantitative evaluation of charge density at the mid bond positions between the atoms given in table 9 also evidences the trend. These pictures show that the charge ordering is taking place when yttrium is doped at the lattice site of La/Sr at the stoichiometric composition  $x = 0.2$  and this result is also supported by the angular arrangement of La–O–La and Mn–O–Mn as discussed earlier. And hence it may be

**Table 7.** Charge density at the bond critical point.

Bond	$x = 0$		$x = 0.1$		$x = 0.2$		$x = 0.3$	
	$r (\text{\AA})$	$\rho (\text{e}/\text{\AA}^3)$	$r (\text{\AA})$	$\rho (\text{e}/\text{\AA}^3)$	$r (\text{\AA})$	$\rho (\text{e}/\text{\AA}^3)$	$r (\text{\AA})$	$\rho (\text{e}/\text{\AA}^3)$
La–O	1.31783	0.45987	1.32043	0.43541	1.32063	0.42696	1.28726	0.47099
Mn–O	1.05268	0.77658	1.05299	0.78785	1.05939	0.75139	1.03011	0.97814
O–O	1.40394	0.30773	1.38842	0.30180	1.39170	0.28849	1.31223	0.37780

assumed that material goes from insulator to metal state at  $x = 0.2$ . This may also be the reason for the weakening of the ferromagnetic order and increasing of the magnetic disorder owing to the presence of yttrium. Thus it is understood that the Y doping imposes charge delocalization and it reflects also on the weakening of the ferromagnetic order and the insulator–metal transition. Thus charge density determination can give minute details on the localization/delocalization of charges in the materials that results in the change in their physical and chemical properties.

## 6. Conclusions

Yttrium doped LSMO prepared using sol–gel technique is analysed for the effect of stoichiometric inclusion of dopant in the charge density distribution in the unit cell using Rietveld and MEM technique. The bonding between the atoms is analysed quantitatively and qualitatively. This results in insulator–metal transition at  $x = 0.2$  that have been studied through charge density distribution analysis for the first time. Such studies can be done to understand the charge ordering behaviour in materials that behave differently when different dopants are included in different magnetic materials.

## References

- Alexandrov A S and Bratkovsky A M 1999 *Phys. Rev. Lett.* **82** 141  
 Anderson P W 1958 *Phys. Rev.* **109** 1498  
 Arima T, Tokura Y and Torrance J B 1993 *Phys. Rev.* **B48** 17006  
 Banach G, Tyer R and Temmerman W M 2004 *J. Magn. Magn. Mater.* **272–276** 1963  
 Bindu R, Maiti Kalobaran, Rawat R and Khalid S 2008 *Appl. Phys. Lett.* **92** 121906  
 Collins D M 1982 *Nature* **49** 298  
 Gaur Anurag and Varma G D 2006 *J. Phys. Condens. Matter* **18** 8837  
 Howard C J 1982 *J. Appl. Crystallogr.* **15** 615  
 Israel S, Saravanan R, Srinivasan N and Rajaram R K 2003 *J. Phys. Chem. Solids* **64** 43  
 Israel S, Saravanan R and Rajaram R K 2004 *Physica* **B349** 390  
 Izumi F and Dilanian R A 2002 *Recent research developments in physics, Part II* (Trivandrum: Transworld Research Network) **3** pp 699–726  
 Janker G H and van Santen J H 1950 *Physica* **16** 337  
 Krishnan K M and Ju H L 1999 *Phys. Rev.* **B60** 14793  
 Livesay E A et al 1999 *J. Phys. Condensed Matter* **11** L2711  
 Lyu P, Xing D Y and Dong J 1998 *Phys. Rev.* **B58** 54  
 Maezono R, Ishihara S and Nagaosa N 1998 *Phys. Rev.* **B58** 11583  
 Momma K and Izumi F 2008 *J. Appl. Crystallogr.* **41** 653  
 Mott N F 1974 *Metal–insulator transitions* (London: Taylor and Francis)  
 Nadgorny B et al 2001 *Phys. Rev.* **B63** 184433  
 Nagarajan 2008 *Nature Mater.* **7** 391  
 Petricek V, Dusek M and Palatinus L JANA 2000 The crystallographic computing system, Institute of Physics, Academy of Sciences of the Czech Republic, Praha  
 Pickett W E and Singh D J 1997 *J. Magn. Magn. Mater.* **172** 237  
 Renuretsen R 2007 *Preparation and characterization of yttrium doped LSMO*, M. Phil. Thesis, The American College, Madurai Kamaraj University, Madurai  
 Rietveld H M 1969 *J. Appl. Crystallogr.* **2** 65  
 Ruben A D and Fujio I 2004 *Super-fast program PRIMA for maximum-entropy method* (Ibaraki, Japan: National Institute for Materials Science) p. 305  
 Saitoh T, Bocquet A E, Mizokawa T, Namatame H, Fujimori A, Abbate M, Takeda Y and Takano M 1995 *Phys. Rev.* **B51** 13942  
 Syed Ali K S, Saravanan R, Israel S and Rajaram R K 2006 *Bull. Mater. Sci.* **29** 107  
 Thompson P, Cox D E and Hastings J B 1987 *J. Appl. Crystallogr.* **20** 79  
 Tokura Y (ed.) 2000 *Colossal magnetoresistive oxides* (New York, USA: Gordon and Breach Science Publishers)  
 Tokura Y and Tomioka Y 1999 *J. Magn. Magn. Mater.* **200** 1  
 Tsai M-H, Tang Y-H, Chou H and Wu W T Private publication submitted to National Science Council of Taiwan  
 Urushibara A, Moritomo Y, Arima T, Asamitsu A, Kido G and Tokura Y 1995 *Phys. Rev.* **B51** 14103  
 Vachhani P S, Solanki P S, Markna J H, Parmar R N, Bhalodia J A and Kuberkar D G 2007 *Indian J. Eng. & Mater. Sci.* **14** 163  
 van den Brink J, Khaliullin G and Khomskii D 1999 *Phys. Rev. Lett.* **83** 5118  
 van Santen J H and Janker G H 1950 *Physica* **16** 599  
 Wertheim G K, Butler M A, West K W and Buchanan D N E 1974 *Rev. Sci. Instrum.* **45** 1369  
 Xiong X, Dabrowski B, Chmaissem O, Bukowski Z, Kolesnik S, Dybzinski R, Kimball C W and Jorgensen J D 1999 *Phys. Rev.* **B60** 10186  
 Yakel H L 1955 *Acta Crystallogr.* **8** 394  
 Zheng R K, Wang Y, Chan H L W, Choy C L and Luo H S 2007 *Appl. Phys.* **90** 152904